

18 **Abstract**

19 Tropospheric ozone pollution in South Asia is mainly blamed on anthropogenic emissions.
20 However, based on ERA5 reanalysis data, this study highlights the contribution of stratospheric
21 ozone intrusions into the Upper Troposphere and Lower Stratosphere (UTLS) associated with
22 Sudden Stratospheric Warming (SSW) events in enhancing upper tropospheric ozone over the
23 South Asian region. We report an enhancement in ozone in the UTLS by more than 80% for
24 2018 and ~30% within ± 6 days of the onset during SSW events concurrent with the westerly
25 phase of Quasi-biennial oscillation (QBO-SSW) compared to non-SSW years. The
26 equatorward shift (south of 30°N) of the subtropical jet during QBO-SSW causes lowering of
27 the tropopause and more Rossby-wave breaking in the upper troposphere. This results in higher
28 stratospheric ozone intrusions over the South Asian region. The ozone enhancement during
29 QBO-SSW events produces an instantaneous radiative forcing at the top of the atmosphere of
30 $0.09 \pm 0.05 \text{ W.m}^{-2}$ due to UTLS ozone changes and $0.17 \pm 0.05 \text{ W.m}^{-2}$ from total-column ozone
31 changes over South Asia.

32 **Keywords:** Sudden stratospheric warming, stratosphere intrusions, ozone radiative forcing, South
33 Asian region, Rossby wave breaking.

34

35

36

37

38 1. Introduction

39 Tropospheric ozone is a short-lived greenhouse gas that plays a crucial role in
40 atmospheric chemistry and radiative forcing (Wang et al., 2022). It is also a major air pollutant
41 that significantly affects human health (Lim et al., 2012; Fleming et al., 2018), damages
42 vegetation (Feng et al., 2021), disrupts ecosystems, and imposes economic costs (Dewan and
43 Lakhani, 2022). In South Asia, a significant amount of tropospheric ozone is a growing concern
44 due to its increased hazardous health effects (Lin et al., 2018).

45 The contribution from the downward transport of ozone-rich air from the stratosphere is
46 the largest natural source of tropospheric ozone (e.g., Fadnavis et al., 2010; Roy et al., 2020).
47 Studies have reported that stratospheric influence on the tropospheric ozone exceeds 50% in the
48 winter season at the extratropics (Williams et al., 2019). Wang and Fu (2021) estimate that
49 stratosphere-to-troposphere exchange (STE) contributes approximately 347 ± 12 Tg year⁻¹ to the
50 global tropospheric ozone budget based on both observations and reanalysis data. CMIP6 model
51 simulations for the period 1997 to 2014 indicate that up to 30% of surface ozone in the Northern
52 Hemisphere during winter (DJF) is due to stratospheric ozone intrusions (Li et al., 2024). In the
53 Northwest Pacific, STE increases mid and upper-tropospheric ozone by about 96% in winter and
54 40% in summer between 1990 and 2020 (Ma et al., 2024). Roy et al. (2023) reported an ozone
55 enhancement of ~40 ppb in the upper troposphere over the Indian region caused by stratospheric
56 intrusions associated with tropical cyclones.

57 Sudden stratospheric warming (SSW) events play a key role in atmospheric dynamics
58 and stratospheric ozone intrusions into the troposphere (e.g., Williams et al., 2024). SSWs are
59 one of the most significant large-scale dynamical phenomena in the stratosphere during winter
60 (Butler et al., 2015; Baldwin et al., 2021). Enhanced planetary wave activity from the

61 troposphere disrupts the stratospheric polar vortex, decelerating or even reversing the
62 stratospheric westerlies, and causing a rapid rise in polar stratospheric temperatures by up to 50
63 K within few days (Baldwin et al., 2021). SSW events are crucial in modulating extreme heat, air
64 pollution, wildfires, wind extremes, storm clusters, tropical cyclones, and sea ice melt in the
65 northern high latitudes (Domeisen and Butler, 2020; Domeisen et al., 2020). The temperature
66 and wind anomalies associated with SSWs propagate downward into the troposphere over
67 timescales ranging from weeks to months, impacting tropospheric weather in the Northern
68 Hemisphere for up to 40 days following the onset of the event (Baldwin and Dunkerton, 2001;
69 Hall et al., 2021). Studies also suggest that SSWs are often followed by an equatorward shift of
70 the tropospheric jet stream and storm tracks, as well as surface pressure anomalies that resemble
71 the negative phase of the Northern Annular Mode (Sigmond et al., 2013; Kidston et al., 2015).
72 Projection studies suggest that SSW events will increase by approximately one event per decade
73 by the end of the 21st century (Charlton-Perez et al., 2008). High greenhouse gas emission
74 scenarios indicate a doubling in SSW frequency (Schimanke et al., 2012). Considering the
75 frequent occurrences and the potential role of SSWs in STE, it is important to investigate SSWs
76 influence on tropospheric ozone enhancements and the associated radiative effects.

77 SSW events have a significant influence on STE and impact the tropospheric ozone
78 budget, particularly in high-latitude regions (Xia et al., 2023; Williams et al., 2024; Lee et al.,
79 2025). Based on 11 polar-night jet oscillation (PJO) type SSW events from 1980 to 2013 and
80 chemistry-climate model simulations, STE led to an average increase of 5–10% in near-surface
81 ozone over the Arctic (Williams et al., 2024). Xia et al. (2023) reported an even more
82 pronounced increase of 76% in Arctic surface ozone due to STE in the 2020/21 SSW event.
83 While most of these studies focus on the polar regions, some have identified SSW-induced ozone

84 variability in the mid-latitudes (Liu et al., 2009; Williams et al., 2024). Liu et al. (2009) noted an
85 ozone enhancement of about 186 Tg in the upper troposphere over East Asia during the 2002–
86 2003 SSW, using MOZART-3 simulations. However, tropospheric ozone variations during SSW
87 events over South Asia are among the least studied. Additionally, the broader implications of
88 these events on the ozone radiative forcing over this region remain largely underexplored.

89 In this study, we investigate the impact of all the SSW events from 1962 to 2018 on
90 ozone variability in the upper troposphere and lower stratosphere (UTLS: 300-50 hPa) over the
91 South Asian region (20-35°N, 65-90°E) using ERA5 reanalysis data. The composite is obtained
92 by averaging data with the onset day as a central date (details in the ‘Methods’ section). A recent
93 study by Shi et al. (2023) reported that during the 2018 SSW over East Asia, surface
94 temperatures dropped by up to $\sim 18^{\circ}\text{C}$ relative to pre-event conditions. However, to our
95 knowledge, UTLS ozone responses over South Asia during this event have received limited
96 attention, which motivates our emphasis on the 2018 case. We further extend the analysis to all
97 SSWs and assess their contribution to upper-tropospheric ozone and regional ozone radiative
98 forcing.

99 The paper is organised as follows. Section 2 describes the ERA5 reanalysis dataset, and
100 the computation of ozone radiative forcing using the radiative-kernel method. Section 3 presents
101 the (i) UTLS ozone changes during the 2018 SSW event over South Asia, (ii) composite analysis
102 of SSWs, and (iii) ozone radiative forcing. Section 4 summarises the main findings.

103 **2. Methods**

104 **2.1 ERA 5 Reanalysis Data**

105 We analysed daily data of ozone, zonal and meridional winds, geopotential height (GPH),
106 and potential vorticity (PV) from the fifth-generation reanalysis dataset (ERA5) provided by the

107 European Centre for Medium-Range Weather Forecasts (ECMWF) (Hersbach et al., 2020). The
108 ERA5 ozone field is generated through assimilation of multiple satellite- and ground-based
109 observations, including TOMS (1978–2006), SBUV v8.6 (1978–present), CCI MIPAS (2005–
110 2012), SCIAMACHY (2002–2012), Aura MLS v4.2 (2004–present), and OMI-DOAS (2004–
111 present) (Hersbach et al., 2020; S-RIP Final Report, 2022). Comparison of ERA5 ozone with
112 observations shows a slight overestimation in the UTLS. For example, over the North India
113 region, ERA5 shows an overestimation of ~20 ppb ozone (Fadnavis et al., 2023). However,
114 ERA5 ozone showed lesser biases compared to other reanalyses (Fadnavis et al., 2023). The S-
115 RIP (2022) assessment report states an overestimation of zonal mean ozone by ~10–40%
116 between 50°N and 50°S. The ERA5 variables have a horizontal resolution of $0.25^\circ \times 0.25^\circ$
117 across 37 standard pressure levels (1000 to 1 hPa). Composite analysis is conducted for all
118 variables for ± 30 days, centered on the onset of SSW events (30 days before and after the onset),
119 to assess the impact.

120 Daily anomalies in ozone, geopotential height, winds, and PV during the SSW days were
121 calculated by subtracting the corresponding calendar-day climatology, computed from all the
122 non-SSW years. The long-term trend is removed from the daily ERA5 data before computing
123 anomalies. This approach ensures that anomalies reflect deviations from typical background
124 conditions. To determine statistical significance, we used the Monte Carlo bootstrap and the
125 Wilcoxon signed-rank test. For the Monte Carlo, we built a calendar-matched non-SSW
126 background ensemble by resampling days from non-SSW years within the same day-of-year
127 window (20,000 resamples). We then use a bias-corrected and accelerated (BCa) bootstrap with
128 20,000 resamples to form 95% confidence intervals. For 2018, we checked whether the observed
129 value lay outside the BCa interval of the background ensemble. For the composite, we computed

130 the event composite mean and tested it against the distribution of composite means obtained
131 from the same non-SSW background ensemble (20,000 resamples). A grid point was considered
132 significant if the event composite mean lay outside the 95% BCa confidence interval of this
133 background distribution. Next, we applied an exact Wilcoxon signed-rank test to the same data.
134 A grid point is considered significant only when both tests agree at 95% significance.

135 The onset of all the SSW events is identified as the day when the zonal mean westerly
136 winds at 10 hPa and 60°N reverse their direction from westerlies to easterlies (Charlton and
137 Polvani 2007). Figure S1 shows the temporal evolution of the zonal-mean zonal wind at 60° N
138 and 10 hPa for the 2018 SSW event. To diagnose stratospheric intrusions, we use potential
139 vorticity (PV) as a dynamical tracer of stratospheric air and adopt the 2-PVU contour as a proxy
140 for the dynamical tropopause (e.g., Kunz et al., 2011; Holton et al., 1995). Intrusions are
141 identified from PV streamers or tropopause folds when high-PV (≥ 2 PVU) extends equatorward
142 and downward into the upper troposphere (e.g., Sprenger et al., 2007). To demarcate the
143 boundary between the troposphere and stratosphere, we used the WMO lapse-rate tropopause
144 (WMO 1957). We used the lapse rate tropopause (LRT) derived from the ERA5 data for the
145 present study (Hoffmann and Spand 2022). This definition is adopted to mark a temporally
146 varying troposphere–stratosphere boundary that is consistent with the dynamical changes.
147 Further, phases of the Quasi-biennial oscillation (QBO) are identified using zonal-mean zonal
148 wind data from radiosonde observations published by the Freie Universität Berlin. The
149 classification of westerly and easterly QBO phases is based on winds at 70 hPa. Periods with
150 positive zonal wind values (>0 m.s⁻¹) are identified as the westerly QBO (WQBO), while periods
151 with negative zonal wind values (<0 m.s⁻¹) are classified as the easterly QBO (EQBO).

152

153 **2.2 Computation of ozone radiative forcing**

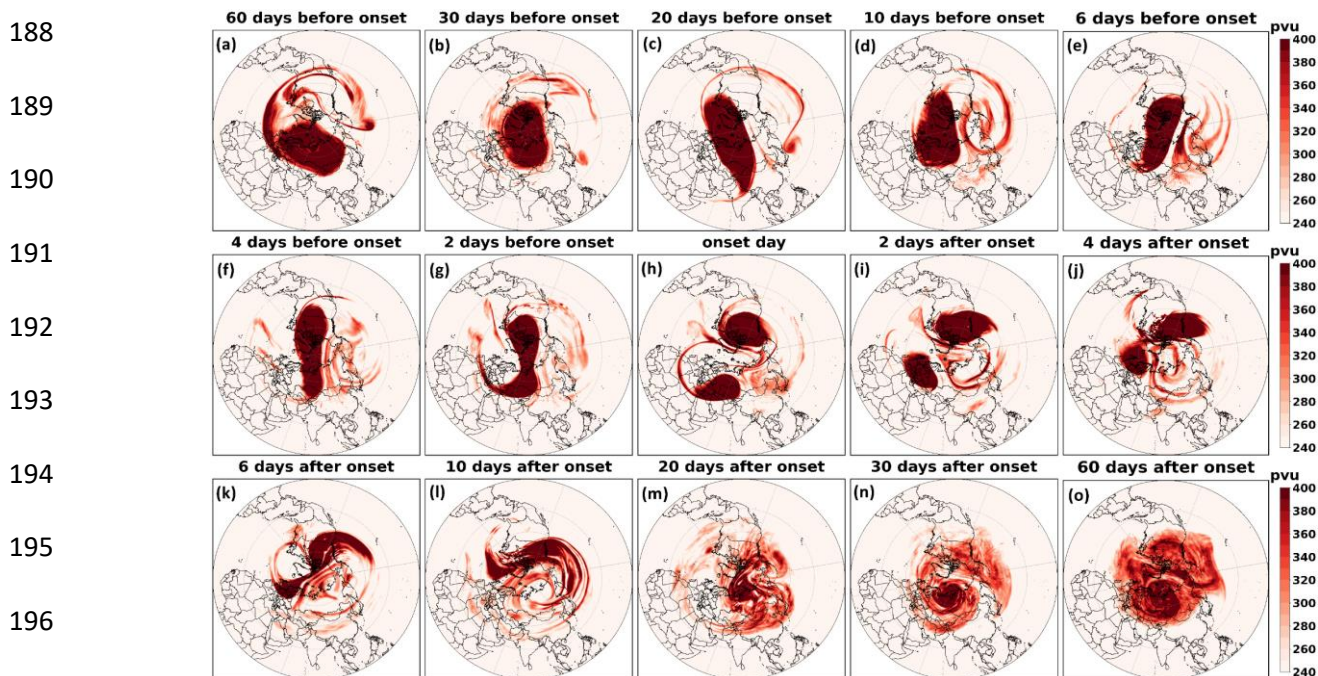
154 The ozone radiative forcing (RF) is estimated using an ozone radiative kernel method
155 (Skeie et al., 2020). The radiative kernel is constructed using the University of Oslo radiative
156 transfer model (Myhre et al., 2011) by perturbing the ozone layer-by-layer. Temperature, water
157 vapour, and clouds are incorporated into the model from ECMWF's forecast for the year 2003
158 and applied as monthly averages. The model calculates radiative forcing using a broad-band
159 scheme for longwave radiation (Myhre and Stordal, 1997) and the DIScrete Ordinate Radiative
160 Transfer (DISORT) code for shortwave radiation (Stamnes et al., 1988). Previous studies have
161 shown that the ozone radiative forcing estimates from the radiative kernel technique and a
162 radiative transfer model agree within 0.01 W.m^{-2} globally (Iglesias-Suarez et al., 2018). Before
163 applying the kernel, the ERA5 ozone data are linearly interpolated to the kernel resolution ($\sim 5.6^\circ$
164 $\times 5.6^\circ$ horizontal, with 60 vertical levels). The interpolated ozone fields are first converted into
165 layer-wise partial column amounts in Dobson units (DU) following Ziemke et al. (2001). Ozone
166 anomalies in DU are then computed from the non-SSW climatology at each grid point. These
167 layer-wise DU anomalies are multiplied by the long-wave instantaneous clear-sky ozone kernel
168 ($\text{W.m}^{-2}.\text{DU}^{-1}$), which gives the change in top-of-atmosphere (TOA) long-wave radiative flux
169 (defined as an increase in net downward flux; $\Delta (F_{\text{in}} - F_{\text{out}}) > 0$) per DU of ozone change in each
170 layer. Following Shell et al. (2008), we calculate the instantaneous ozone RF by vertically
171 summing the layer-wise TOA contributions from the UTLS and the total atmosphere.

172 **3. Results**

173 **3.1 Polar vortex evaluation in 2018 SSW event**

174 The time evolution of the vortex structure depicted by PV at 10 hPa for ± 30 days around
175 the 2018 SSW onset is shown in Fig. 1. As the SSW event approaches, the vortex begins to

176 elongate and become asymmetrical (Fig. 1a-g) due to the influence of planetary wave activity
 177 propagating upward from the troposphere; such deformation of the vortex was reported in the
 178 past (e.g., Baldwin et al., 2021). On the onset day (12 February), the vortex splits into two high-
 179 PV lobes, one positioned over North America and another over Eurasia (Fig. 1h). Following the
 180 onset, smaller vortices exhibit swirling and filamentation, with the Eurasian lobe drifting
 181 westward (Fig. 1i-j). Polar vortex splitting or deformations cause equatorward meandering of
 182 upper tropospheric jet that affect the Rossby wave breaking (RWB) and ozone intrusions in the
 183 mid-latitudes (Baldwin et al., 2021; Albers et al., 2015). The equatorial meandering of the jet
 184 may influence the tropical region; however such analysis is sparse. In the following sections we
 185 show the influence of the 2018 SSW on the South Asian region. First we show ozone variation in
 186 the UTLS over South Asia and then explain the associated dynamical changes in RWB and the
 187 upper tropospheric jet.



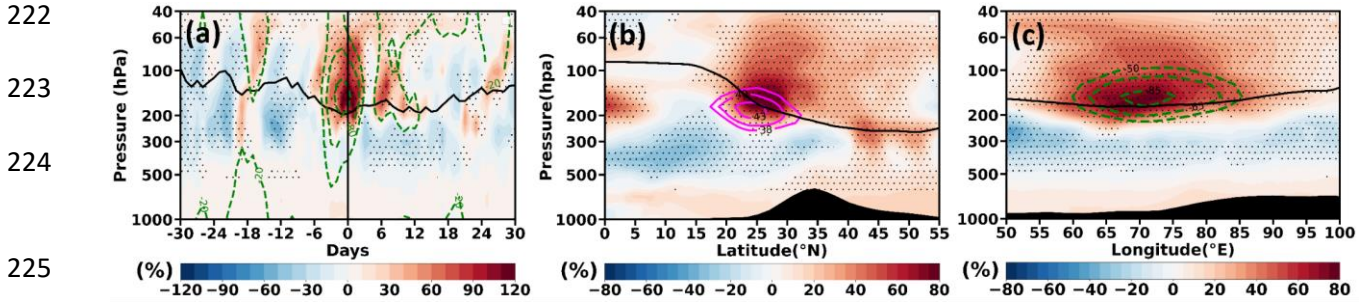
197 **Figure 1.** Time slice of the spatial distribution of potential vorticity (PV) at 10 hPa from 30 days
 198 before to 30 days after the onset of the 2018 SSW event.

199 3.2 February 2018 SSW case: UTLS ozone variation

200 Figures 2a show the vertical distribution of the temporal evolution of ozone anomalies
201 averaged over South Asia for the 2018 SSW event. There is a large ozone enhancement in the
202 UTLS, with values $>80\%$ (>150 ppb) in 2018 within ± 6 days around the SSW onset. Figure 2a
203 indicates that the ozone enhancements in the UTLS region coincide with negative geopotential
204 height (GPH) anomalies. Since the most pronounced ozone enhancement in the UTLS is
205 observed within ± 6 days around the SSW onset, all subsequent analyses in this study are
206 performed for this time period. The latitude–pressure (Fig. 2b) and longitude–pressure (Fig. 2c)
207 cross-sections of ozone anomalies show large ozone enhancement for ± 6 days around the onset
208 in the UTLS over South Asia, exceeding 60% (>80 ppb). Interestingly, a peak in ozone
209 enhancement is seen at the subtropical jet core (Fig.2b). This suggests the role of the subtropical
210 jet causing ozone enhancement in the upper troposphere over South Asia. The strong negative
211 GPH anomaly (indicating a low-pressure area) coincident with large ozone enhancements
212 provides evidence of stratospheric intrusions occurring during the 2018 SSW event (Fig. 2c). In
213 addition, the reduced tropopause height near the onset in Fig.2a suggests the occurrence of
214 tropopause folds. Earlier studies have shown that Rossby wave breaking (RWB) produces
215 tropopause folds, providing an efficient pathway for quasi-isentropic descent of ozone-rich
216 stratospheric air into the UTLS (Sprenger et al., 2003; Holtan et al., 1995). Past literature reports
217 ozone enhancements in the polar region associated with SSW (e.g., Baldwin et al., 2021);
218 however, high ozone enhancement in the UTLS over the South Asian region underscores the
219 unique regional impacts of SSWs.

220

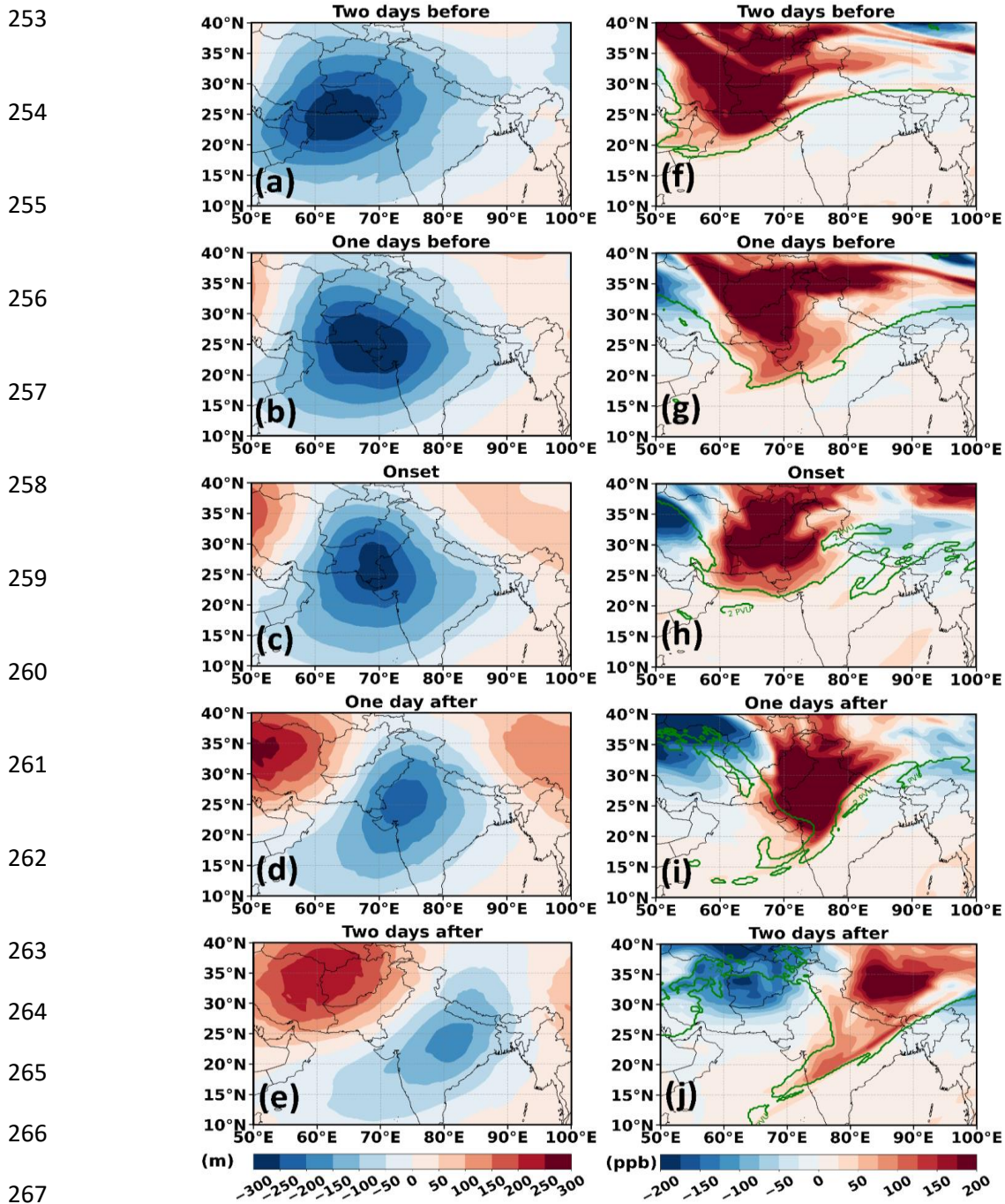
221



226 **Figure 2.** (a) Temporal evolution of vertical ozone anomalies averaged over the South Asian
 227 region (65-90°E, 20-35°N) from 30 days before to 30 days after the onset for the 2018 event. (b)
 228 Latitude-pressure section of ozone anomalies averaged over South Asia (65 - 90°E) for ±6 days
 229 around the onset for 2018 SSW event. (c) is the same as that of (b) but represents longitude
 230 variations of vertical ozone anomalies averaged over South Asia (20-35°N). The vertical solid
 231 black line in (a) represents the onset day. Magenta solid contour lines in (b) represent the mean
 232 zonal wind and green dashed contour lines in (a) and (c) represent the GPH anomaly. Solid black
 233 lines in panels (a-c) represent the lapse rate tropopause. Black dots indicate a region of 95%
 234 confidence level.

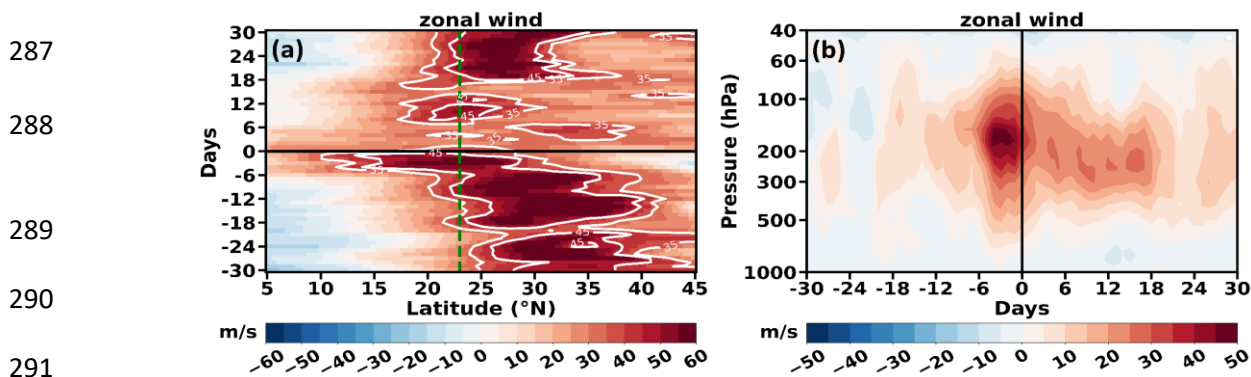
235 Further, we discuss the possible mechanism responsible for the ozone enhancement in the
 236 UTLS over South Asia associated with the 2018 SSW event. Several studies have shown that
 237 SSW-related planetary wave disturbances occur across a deep layer of the stratosphere (e.g.,
 238 Albers et al., 2016). These disturbances extend downward and disrupt horizontal flows in the
 239 upper troposphere (200 hPa) (Albers et al., 2016). To explore the influence of these disturbances
 240 over the South Asian region, we analysed GPH anomalies at 200 hPa. The evolution of GPH
 241 anomalies at 200 hPa for ±2 days around the SSW onset (Feb. 12, 2018) is shown over the South
 242 Asian region in Fig. 3a-e and for the Northern Hemisphere in (Fig. S2a-e). In the Northern
 243 Hemisphere, patterns of high and low GPH anomalies at 200 hPa in the subtropical region (15-
 244 40°N) indicate the presence of synoptic-scale Rossby waves in the upper troposphere (Fig. S2a-
 245 e). The low GPH anomaly over South Asia (also see Fig. 3a-e) indicates a low-pressure area
 246 causing deepening of trough. It is associated with the eastward propagation of Rossby waves,
 247 which can facilitate enhanced stratospheric intrusions. RWB is characterised by large filaments
 248 of high-potential vorticity (PV) air extending towards the equator. The 2 PVU contour lines,

249 along with ozone anomaly maps at 200 hPa, depicted in Fig. 3f-j show clear indications of RWB
 250 causing ozone intrusions over South Asia. Such quasi-isentropic equatorward excursions cause
 251 irreversible ozone intrusion from the lower stratosphere into the upper troposphere (e.g., Holton
 252 et al., 1995;-Waugh and Polvani, 2000).



268 **Figure 3.** Spatial map of (a-e) GPH anomaly at 200 hPa, (f-j) ozone anomaly at 200 hPa from 2
 269 days before to 2 days after the onset of the 2018 SSW event, along with 2 PVU contour (green
 270 solid line), shown at 1-day intervals.

271 Figures 3f-j clearly show that intrusions near SSW onset days cause large ozone
 272 enhancements >150 ppb ($>80\%$) over South Asia. Since the location and strength of the
 273 subtropical jet set the refractive waveguide and the location of wave breaking (Hoskins &
 274 Ambrizzi 1993; Hitchman & Huesmann 2007), we next diagnose the jet's evolution during this
 275 period. Figure 4 displays the latitude-time Hovmöller diagrams of zonal wind at 200 hPa and the
 276 time-altitude section around the onset over the South Asian region. Figure 4 clearly shows the
 277 equatorward shift of the subtropical jet around onset, creating the background flow conducive to
 278 the RWB and ozone intrusions seen in Fig. 3. The time evolution of zonal winds depicted in
 279 Figure 4a shows that thirty days before the onset, the subtropical jet core is positioned over the
 280 northern part of the Indian subcontinent, and migrates equatorward (south of 23°N) more
 281 prominently for ± 6 days around the onset. The vertical variation of zonal wind (Fig. 4b) also
 282 indicates an equatorward displacement of the subtropical jet, with enhanced westerlies near 200
 283 hPa extending into $10\text{--}20^{\circ}\text{N}$ over $65\text{--}90^{\circ}\text{E}$ around the onset day. Such changes in jet structure
 284 are consistent with a stronger upper-tropospheric Rossby-wave waveguide and background
 285 conditions under which RWB is more likely to occur near the tropopause (Hoskins and Ambrizzi
 286 1993; Homeyer and Bowman 2013).



292 **Figure 4.** (a) Latitude-time plot of zonal wind averaged over South Asia (65° - 90° E) at 200
293 hPa. (b) Temporal evolution of vertical zonal wind averaged over the South Asian region (65 -
294 90° E, 10 - 20° N) for ±30 days around the onset of the 2018 SSW event. The horizontal solid
295 line in (a) and the vertical solid line in (b) represent the onset day. The vertical dashed line in (a)
296 represents 23°N.

297 The observed equatorward shift of the subtropical jet during the 2018 SSW may also be
298 influenced by the concurrent phase of the Quasi-Biennial Oscillation (QBO) (e.g., White et al.,
299 2016; Li et al., 2023). Notably, the February 2018 SSW took place during the westerly phase of
300 the QBO (Butler et al., 2020). Earlier studies have reported an equatorward shift of the
301 subtropical jet over the East Asia–North Pacific region during the westerly phase of QBO (Park
302 et al., 2021). Our analysis reveals a similar equatorward displacement of the subtropical jet over
303 South Asia during SSWs (Fig. 4a), coinciding with the westerly QBO phase. During the
304 westerly QBO, the associated secondary circulation warms the equatorial lower stratosphere and
305 cools the subtropics, sharpening and shifting the UTLS meridional temperature gradient
306 equatorward (e.g., Hitchman et al., 2021). By thermal-wind balance, this strengthens upper-
307 tropospheric westerlies on the equatorward flank and displaces the subtropical jet equatorward
308 over South Asian longitudes, favouring subtropical wave guidance, RWB, and PV-streamer
309 intrusions (Homeyer & Bowman, 2013; Albers et al., 2016). Additionally, previous studies have
310 shown that the westerly phase of QBO (WQBO) is associated with a lowering of the tropopause
311 (Collimore et al., 2003; Kumar et al., 2014). This lowering perturbs the subtropical waveguide
312 structure and enhances tropopause fold activity (Kumar et al., 2020), thereby increasing the
313 frequency of Rossby wave breaking and strengthening stratosphere–troposphere exchange,
314 causing enhanced ozone intrusions.

315

316

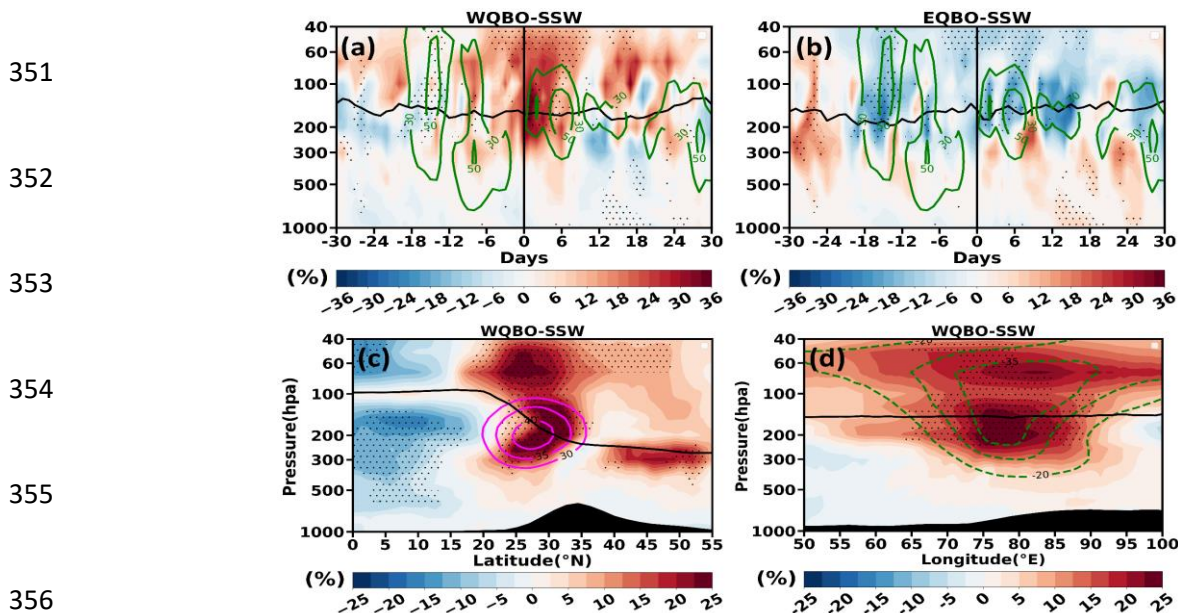
317 **3.3 Composite UTLS Ozone Response during all SSW Events**

318 Further, we investigate the twenty-seven major SSW events from 1962 to 2017, to
 319 examine their influence on ozone variability in the upper troposphere over the South Asian
 320 region. Motivated by the 2018 case study, we examined whether the QBO-phase dependence is
 321 evident across events. Table 1 lists all the major SSW events considered in this study along with
 322 their QBO phases. Of the 27 major SSWs, 15 occur during the westerly phase (WQBO-SSW)
 323 and 12 during the easterly phase (EQBO-SSW).

324 **Table 1.** List of all major SSW events from 1962 to 2018 considered for the present analysis
 325 alongside their onset dates and QBO phases at 70 hPa.

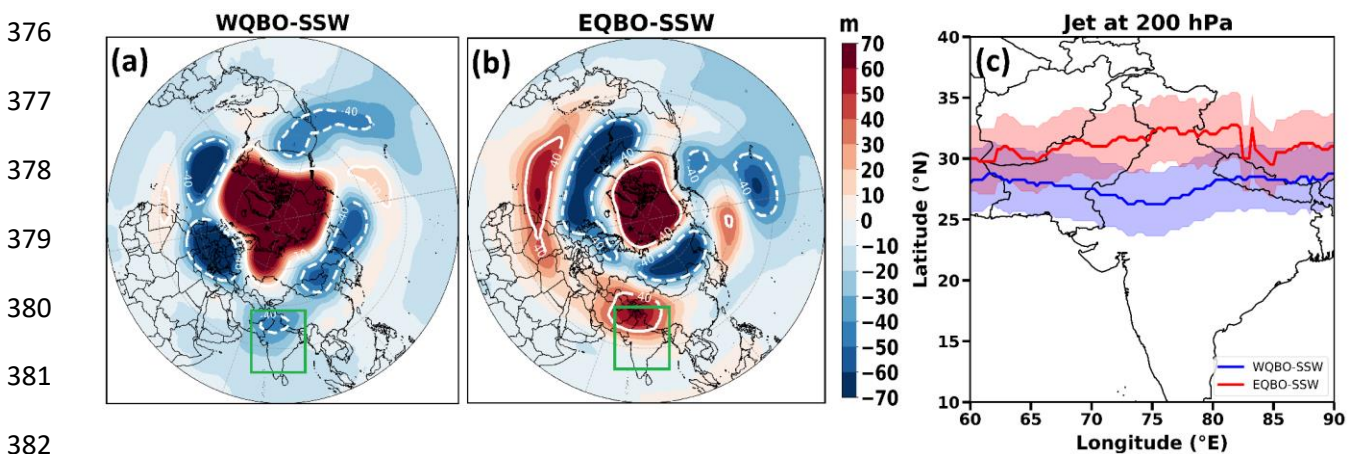
Year	Onset day	QBO Phase
1963	28 January	Westerly
1966	23 February	Easterly
1968	7 January	Westerly
1969	13 March	Easterly
1970	2 January	Westerly
1971	18 January	Easterly
1973	31 January	Easterly
1977	9 January	Westerly
1979	22 February	Westerly
1980	29 February	Easterly
1981	4 March	Westerly
1984	24 February	Westerly
1985	1 January	Easterly
1987	23 January	Westerly
1988	14 March	Westerly
1989	21 February	Westerly
1999	26 February	Easterly
2000	20 March	Westerly
2001	11 February	Westerly
2003	18 January	Westerly
2004	5 January	Easterly
2006	21 January	Easterly
2007	24 February	Westerly
2008	22 February	Easterly
2009	24 January	Easterly
2010	9 February	Westerly
2013	6 January	Easterly
2018	12 February	Westerly

336 Previous studies have shown that the QBO phase can modulate the dynamical coupling
 337 between the stratosphere and troposphere during SSWs (Remya et al, 2023), influencing the
 338 extent of ozone transport into the upper troposphere (Zhang et al., 2021). Our analysis shows
 339 that, during the composite WQBO-SSW events, ozone intrudes down to 400 hPa, with anomalies
 340 exceeding $\sim 30\%$ (over 80 ppb) within ± 6 days of the onset (Fig. 5a). On the other hand, during
 341 the composite EQBO-SSW events, no significant ozone intrusion is evident within the same
 342 period (Fig. 5b). The latitude–pressure (Fig. 5c) and longitude–pressure (Fig. 5d) sections for
 343 WQBO-SSW further reveal enhanced ozone in the UTLS within ± 6 days over South Asia, with
 344 anomalies exceeding 20% (>60 ppb). As seen earlier (Fig. 2b-c), the maximum ozone
 345 enhancement in the WQBO–SSW composite is located near the subtropical jet core (Fig. 5c)
 346 along with a strong negative GPH anomaly (Fig. 5d), indicating that jet dynamics and troughing
 347 play a key role in modulating UTLS ozone responses during WQBO-SSW. The enhancement in
 348 mean ozone of all WQBO-SSW composite is smaller than in 2018, since there is variation in
 349 space and time of ozone intrusions during individual SSW. The averaging across multiple events
 350 may subdue the effect but it remains statistically significant over South Asia.



357 **Figure 5:** Temporal evolution of vertical ozone anomalies averaged over the South Asian region
 358 (65-90°E, 20-35°N) from 30 days before to 30 days after the onset for (a) WQBO-SSW and (b)
 359 EQBO-SSW. (c) Latitude-pressure cross-section of ozone anomalies averaged over South Asia
 360 (65 - 90°E) for ± 6 days around all the WQBO-SSW onsets. (d) is the same as that of (c) but
 361 represents the longitude variation of vertical ozone anomalies averaged over South Asia (20 -
 362 35°N). The vertical solid line in (a-b) represents the onset day. Magenta contour lines in (c)
 363 represent the mean zonal wind, and dashed green contour lines in (a,d) represent the negative
 364 GPH anomaly and solid green contour lines in (b) represent the positive GPH anomaly. Solid
 365 black lines in (a-d) represent the lapse rate tropopause. Black dots indicate a region of 95%
 366 confidence level.

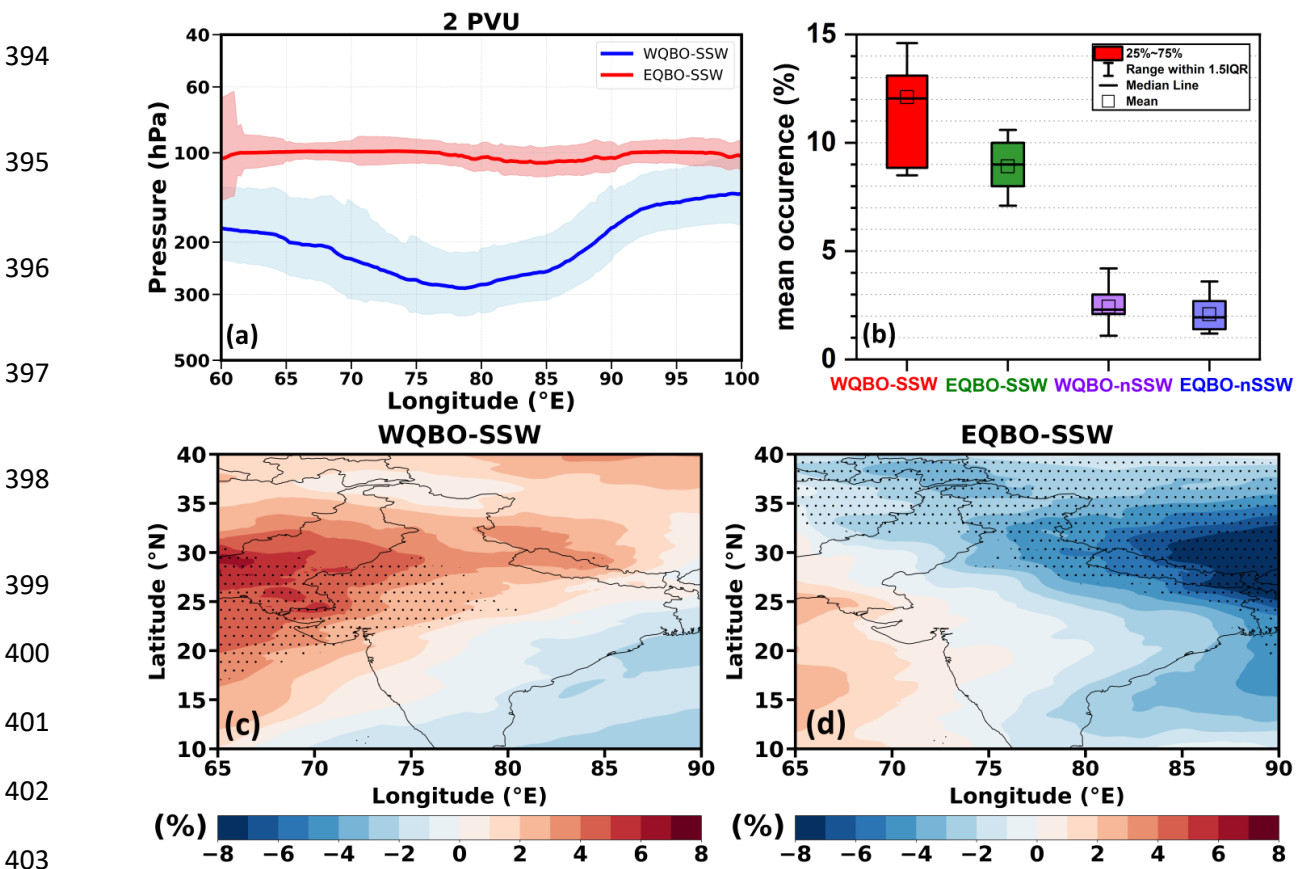
367 Further, we analysed the synoptic wave structure prevailing in the upper troposphere for
 368 WQBO-SSW and EQBO-SSW composites within ± 6 days around the onset, using the 200 hPa
 369 GPH anomaly as a proxy (Figs. 6a–b). The alternating trough–ridge patterns in GPH over the
 370 subtropics indicate synoptic-scale Rossby waves in the upper troposphere. During the WQBO-
 371 SSW a pronounced low GPH anomaly is observed over the South Asian region (Fig. 6a),
 372 whereas high GPH dominates during the EQBO-SSW (Fig. 6b). The anomalous low over South
 373 Asia during WQBO-SSW events indicates a deepening of the upper-tropospheric trough, which
 374 favours the tropopause folding and associated stratospheric intrusions into the upper troposphere
 375 (e.g., Knowland et al., 2017; Sprenger et al., 2007).



383 **Figure 6.** Spatial map of GPH anomaly for (a) WQBO-SSW and (b) EQBO-SSW and (c) jet
 384 core at 200 hPa averaged for ± 6 days around the onset. White solid and dashed contour line in
 385 (a-b) indicates positive and negative GPH anomaly. The square box in (a-b) represents the South
 386 Asian region considered for the present study. Blue line and red line in (c) represents the jet core

387 for westerly phase and easterly phase of QBO respectively. The shading in (c) represents
 388 standard error.

389 Further, we show the position of the subtropical jet core within ± 6 days around the SSW
 390 onset for WQBO-SSW and EQBO-SSW. Figure 6c shows that during WQBO-SSW, the
 391 subtropical jet shifts equatorward, with the jet core (blue lines) located south of 30°N over the
 392 South Asian region. Whereas, during the EQBO-SSW, the jet core (red line) remains north of
 393 30°N . (Detailed mechanism discussed in the section 3.2).



404 **Figure 7.** (a) Longitude-pressure cross section of 2PVU line averaged over South Asia (20-
 405 35°N) for WQBO-SSW and EQBO-SSW composites, shown for the days of maximum intrusion
 406 selected within ± 6 days around the onset. The shading represents standard error. (b) Area-
 407 averaged occurrence frequency (%) of Rossby wave breaking events during January-March over
 408 South Asia identified from $PV > 2$ and Ozone > 80 ppbv at 300 hPa for WQBO-SSW, EQBO-
 409 SSW, WQBO-nonSSW, and EQBO-nonSSW. (c) UTLS ozone anomaly composites (in %) for
 410 ± 30 days around onset for WQBO-SSW relative to WQBO-nonSSW. (d) same as that of (c)
 411 for EQBO-SSW relative to EQBO-nonSSW. Stippling indicates a region of 95% confidence
 412 level.

413 The PV-based RWB diagnostics for composite of WQBO-SSW and EQBO-SSW is
414 shown in Figure 7a. For each event, the day of maximum intrusion within ± 6 days around the
415 onset was chosen to capture the most representative feature, as averaging over the period tends to
416 smooth out the signal. The longitude-pressure cross section (Fig. 7a) shows that during the
417 WQBO-SSW, the 2 PVU contour extends farther downward into the upper troposphere,
418 consistent with more pronounced tropopause folding and PV intrusion signatures. On the other
419 hand, during EQBO-SSW events, the 2 PVU contour remains at higher altitudes, suggesting
420 weaker intrusions.

421 Further, we computed the occurrence frequency of RWB over South Asia during
422 January-March for WQBO-SSW, EQBO-SSW, WQBO-nonSSW, and EQBO-nonSSW. Fig 7b
423 shows the highest occurrence of $\sim 12\%$ for WQBO-SSW, while RWB frequency is less for
424 EQBO-SSW, WQBO-nonSSW, and EQBO-nonSSW. UTLS ozone also shows the highest
425 enhancement for WQBO-SSW. Thus, equatorial shift of sub-tropical jet during WQBO-SSW
426 causes RWB over south Asia leading to large ozone intrusions (Fig. 7d).

427 **3.4 Radiative Forcing of ozone associated with WQBO-SSWs over the South Asian region**

428 Further, we assessed instantaneous radiative forcing at the top of the atmosphere (TOA)
429 due to ozone enhancements in (1) the UTLS and (2) total-column over the South Asian region
430 associated with WQBO-SSW events. The instantaneous RF is computed for ± 6 days around the
431 onset. RF at TOA due to the ozone enhancements in the UTLS is $0.25 \pm 0.18 \text{ W.m}^{-2}$ for the 2018
432 SSW, while the WQBO-SSW composite produces a forcing of $0.09 \pm 0.05 \text{ W.m}^{-2}$.

433 The estimated RF at the TOA due to the total-column ozone changes is $0.28 \pm 0.19 \text{ W.m}^{-2}$
434 for the 2018 event and $0.17 \pm 0.05 \text{ W.m}^{-2}$ for the composite. These results highlight the

435 significant role of WQBO-SSW events in modulating the radiative balance at the TOA over
436 South Asia. These changes in RF will affect UTLS temperature, stability, high clouds, and STE
437 (e.g., Xia et al., 2018; Nowack et al., 2014).

438 **4. Conclusions**

439 Using the ERA5 reanalysis (1962–2018), we investigated the impact of sudden
440 stratospheric warmings (SSWs) on ozone variations in the UTLS (300–50 hPa) over South Asia.
441 Unlike prior global analyses, we demonstrate that SSWs coinciding with the westerly phase of
442 QBO (WQBO-SSW) lead to a substantial enhancement in UTLS ozone and radiative forcing
443 over the South Asian region, whereas SSWs associated with the easterly phase of QBO (EQBO-
444 SSW) do not. Our analysis shows that, unlike high latitudes, the South Asian response is not a
445 direct downward influence. These low-latitude impacts are mediated by Rossby-wave dynamics.
446 In particular, Rossby-wave breaking (RWB) and PV-streamer intrusions develop with the
447 equatorward meandering of the subtropical jet.

448 We find that SSWs coinciding with the westerly phase of the QBO (WQBO-SSW) are
449 associated with an equatorward shift (south of 30°N over South Asia) of the subtropical jet and
450 lowering of tropopause which intensifies RWB and the large ozone anomalies in the UTLS over
451 South Asia. An enhancement in ozone (ranging from 30 to 80% or 80 to 150 ppb for composite
452 and 2018) in the UTLS is noted during the WQBO-SSW years relative to the non-SSW calendar-
453 day climatology within ± 6 days of onset. This ozone enhancement in the UTLS during WQBO-
454 SSW events enhances an instantaneous radiative forcing at the top of the atmosphere by $0.25 \pm$
455 0.18 W.m^{-2} for the 2018 and $0.09 \pm 0.05 \text{ W.m}^{-2}$ during the composite of all WQBO-SSW. Due to
456 total-column ozone changes, instantaneous RF at the top of the atmosphere increases by $0.28 \pm$
457 0.19 W.m^{-2} for 2018 and $0.17 \pm 0.05 \text{ W.m}^{-2}$ for the WQBO-SSW composite. This positive TOA

458 radiative forcing does not necessarily imply surface warming, as ozone perturbations can also
459 induce negative surface radiative forcing. For example, Williams et al. (2024) reported a surface
460 forcing of -0.36 W.m^{-2} associated with ozone changes in the UTLS. Our radiative kernel method
461 does not estimate a surface forcing associated with ozone changes in the UTLS. The
462 enhancements in ozone and associated RF can affect the stability and temperature of the UTLS,
463 high clouds, and the STE. However, such analysis is beyond the scope of the present study.

464 Since the evolution of the polar vortex modulates subtropical Rossby-wave guides that
465 affect South Asia, these stratospheric influences must be represented in regional prediction
466 systems. Earlier studies have shown that using high-top, stratosphere-resolving models improve
467 subseasonal-to-seasonal predictability (Hardiman et al., 2012; Charlton-Perez et al., 2013; Scaife
468 et al., 2022). We emphasise that models should be extended to the stratosphere, including polar
469 vortex dynamics, for accurate sub seasonal-to-seasonal prediction over South Asia.

470

471 **Code and data availability**

472 The ERA5 data that support the findings of this study are openly available from
473 <https://cds.climate.copernicus.eu/> (10.24381/cds.bd0915c6). All the Figures are created using the
474 Python software. The python code used to plot figures in this paper are available from
475 <https://doi.org/10.5281/zenodo.17639489>

476 **Acknowledgements**

477 The authors thank the staff of the High Power Computing Centre (HPC) in IITM, Pune, India,
478 for providing computer resources and the team members of ERA5 for providing data. The
479 authors are thankful to three anonymous reviewers for their valuable suggestions.

480 **Author contributions**

481 Conceptualisation: S.F. Supervision: SF, MH, RF Investigation and methodology: SC, SR, VS,
482 and PC. Writing: all authors.

483 **Competing interests**

484 At least one of the (co-)authors is a member of the editorial board of Atmospheric Chemistry and
485 Physics.

486 **References:**

487 Albers, J. R., Kiladis, G. N., Birner, T. and Dias, J.: Tropical upper-tropospheric potential
488 vorticity intrusions during sudden stratospheric warmings, *Journal of the Atmospheric*
489 *Sciences*, 73(6), 2361–2384, doi:10.1175/jas-d-15-0238.1, 2016.

490 Baldwin, M. P. and Dunkerton, T. J.: Stratospheric harbingers of anomalous weather regimes,
491 *Science*, 294(5542), 581–584, doi:10.1126/science.1063315, 2001.

492 Baldwin, M. P., Domeisen, D. I. V., Hegglin, M. I., Garny, H., Garfinkel, C. I., Langematz, U.,
493 Charlton-Perez, A. J., Butchart, N., Gerber, E. P., Birner, T., Butler, A. H., Ayarzagüena, B.,
494 and Pedatella, N. M.: Sudden Stratospheric Warmings, *Reviews of Geophysics*, 59,
495 <https://doi.org/10.1029/2020rg000708>, 2021.

496 Butler, A. H., Seidel, D. J., Hardiman, S. C., Butchart, N., Birner, T. and Match, A.: Defining
497 sudden stratospheric warmings, *Bulletin of the American Meteorological Society*, 96(11),
498 1913–1928, doi:10.1175/bams-d-13-00173.1, 2015.

499 Butler, A. H., Lillo, S. P., Long, C. S., Lee, S. H., and Lawrence, Z. D.: Differences between the
500 2018 and 2019 stratospheric polar vortex split events, *Quarterly Journal of the Royal*
501 *Meteorological Society*, 146, 3503–3521, <https://doi.org/10.1002/qj.3858>, 2020.

502 Charlton, A. J. and Polvani, L. M.: A new look at stratospheric sudden warmings. part I:
503 Climatology and modeling benchmarks, *Journal of Climate*, 20(3), 449–469,
504 doi:10.1175/jcli3996.1, 2007.

505 Charlton-Perez, A. J., Polvani, L. M., Austin, J. and Li, F.: The frequency and dynamics of
506 stratospheric sudden warmings in the 21st century, *Journal of Geophysical Research:*
507 *Atmospheres*, 113(D16), doi:10.1029/2007jd009571, 2008.

508 Charlton-Perez, A. J., Baldwin, M. P., Shaw, T. A., Hardiman, S., Polvani, L., Shindell, D.,
509 Yoden, S., Gerber, E. P., Manzini, E., Calvo, N., Yukimoto, S., Lott, F., Davis, N. A., Black,
510 R. X., Butler, A. H., Krüger, K., Son, S., Kim, J., Lee, Y., Mcdaniel, B. A., Reichler, T.,

511 Christiansen, B., Watanabe, S., Toohey, M., Sigmond, M., Gillett, N., Wilcox, L., and
512 Birner, T.: On the lack of stratospheric dynamical variability in low-top versions of the
513 CMIP5 models, *Journal of Geophysical Research: Atmospheres*, 118, 2494–2505,
514 <https://doi.org/10.1002/jgrd.50125>, 2013.

515 Collimore, C. C., Huesmann, A., Martin, D. W., Hitchman, M. H., and Waliser, D. E.: On The
516 Relationship between the QBO and Tropical Deep Convection, *Journal of Climate*, 16,
517 2552–2568, [https://doi.org/10.1175/1520-0442\(2003\)016<2552:otrbtq>2.0.co;2](https://doi.org/10.1175/1520-0442(2003)016<2552:otrbtq>2.0.co;2), 2003.

518 Dewan, S. and Lakhani, A.: Tropospheric ozone and its natural precursors impacted by climatic
519 changes in emission and dynamics, *Frontiers in Environmental Science*, 10,
520 [doi:10.3389/fenvs.2022.1007942](https://doi.org/10.3389/fenvs.2022.1007942), 2022.

521 Domeisen, D. I. and Butler, A. H.: Stratospheric drivers of extreme events at the Earth’s surface,
522 *Communications Earth & Environment*, 1(1), [doi:10.1038/s43247-020-00060-z](https://doi.org/10.1038/s43247-020-00060-z), 2020.

523 Domeisen, D. I., Grams, C. M. and Papritz, L.: The role of North Atlantic–European weather
524 regimes in the surface impact of sudden stratospheric warming events, *Weather and Climate
525 Dynamics*, 1(2), 373–388, [doi:10.5194/wcd-1-373-2020](https://doi.org/10.5194/wcd-1-373-2020), 2020.

526 Fadnavis, S., Chakraborty, T., and Beig, G.: Seasonal stratospheric intrusion of ozone in the
527 upper troposphere over India, *Annales Geophysicae*, 28, 2149–2159,
528 <https://doi.org/10.5194/angeo-28-2149-2010>, 2010.

529 Fadnavis, S., Wienhold, F. G., Müller, R., Oelsner, P., Vogel, B., Naja, M., Sonbawne, S.,
530 Dirksen, R., Sagalgile, A., and Peter, T.: Comparison of ozonesonde measurements in the
531 upper troposphere and lower Stratosphere in Northern India with reanalysis and chemistry-
532 climate-model data, *Scientific Reports*, 13, <https://doi.org/10.1038/s41598-023-34330-5>,
533 2023.

534 Feng, Z., Agathokleous, E., Yue, X., Oksanen, E., Paoletti, E., Sase, H., Gandin, A., Koike, T.,
535 Calatayud, V., Yuan, X., Liu, X., De Marco, A., Jolivet, Y., Kontunen-Soppela, S., Hoshika,
536 Y., Saji, H., Li, P., Li, Z., Watanabe, M. and Kobayashi, K.: Emerging challenges of ozone
537 impacts on Asian plants: Actions are needed to protect ecosystem health, *Ecosystem Health
538 and Sustainability*, 7(1), [doi:10.1080/20964129.2021.1911602](https://doi.org/10.1080/20964129.2021.1911602), 2021.

539 Fleming, Z. L., Doherty, R. M., von Schneidemesser, E., Malley, C. S., Cooper, O. R., Pinto, J.
540 P., Colette, A., Xu, X., Simpson, D., Schultz, M. G., Lefohn, A. S., Hamad, S., Moolla, R.,
541 Solberg, S. and Feng, Z.: Tropospheric Ozone Assessment Report: Present-day ozone
542 distribution and trends relevant to human health, *Elementa: Science of the Anthropocene*, 6,
543 [doi:10.1525/elementa.273](https://doi.org/10.1525/elementa.273), 2018.

544 Hall, R. J., Mitchell, D. M., Seviour, W. J. and Wright, C. J.: Tracking the stratosphere-to-
545 surface impact of sudden stratospheric warmings, *Journal of Geophysical Research:*
546 *Atmospheres*, 126(3), doi:10.1029/2020jd033881, 2021.

547 Hardiman, S. C., Butchart, N., Hinton, T. J., Gray, L. J., and Osprey, S. M.: The Effect of a
548 Well-Resolved Stratosphere on Surface Climate: Differences between CMIP5 Simulations
549 with High and Low Top Versions of the Met Office Climate Model, *Journal of Climate*, 25,
550 7083–7099, <https://doi.org/10.1175/jcli-d-11-00579.1>, 2012.

551 Hersbach, H., Bell, B., Berrisford, P., Hirahara, S., Horányi, A., Muñoz-Sabater, J., Nicolas, J.,
552 Peubey, C., Radu, R., Schepers, D., Simmons, A., Soci, C., Abdalla, S., Abellan, X.,
553 Balsamo, G., Bechtold, P., Biavati, G., Bidlot, J., Bonavita, M., De Chiara, G., Dahlgren, P.,
554 Dee, D., Diamantakis, M., Dragani, R., Flemming, J., Forbes, R., Fuentes, M., Geer, A.,
555 Haimberger, L., Healy, S., Hogan, R. J., Hólm, E., Janisková, M., Keeley, S., Laloyaux, P.,
556 Lopez, P., Lupu, C., Radnoti, G., de Rosnay, P., Rozum, I., Vamborg, F., Villaume, S. and
557 Thépaut, J.: The ERA5 global reanalysis, *Quarterly Journal of the Royal Meteorological*
558 *Society*, 146(730), 1999–2049, doi:10.1002/qj.3803, 2020.

559 Hitchman, M. H. and Huesmann, A. S.: A Seasonal Climatology of Rossby Wave Breaking in
560 the 320–2000-K Layer, *Journal of the Atmospheric Sciences*, 64, 1922–1940,
561 <https://doi.org/10.1175/jas3927.1>, 2007.

562 Hitchman, M. H., Tegtmeier, S., Yoden, S., Haynes, P. H., and Kumar, V.: An Observational
563 History of the Direct Influence of the Stratospheric Quasi-biennial Oscillation on the
564 Tropical and Subtropical Upper Troposphere and Lower Stratosphere, *Journal of the*
565 *Meteorological Society of Japan. Ser. II*, 99, 239–267, [https://doi.org/10.2151/jmsj.2021-](https://doi.org/10.2151/jmsj.2021-012)
566 012, 2021.

567 Hoffmann, L. and Spang, R.: An assessment of tropopause characteristics of the ERA5 and era-
568 interim meteorological reanalyses, *Atmospheric Chemistry and Physics*, 22(6), 4019–4046,
569 doi:10.5194/acp-22-4019-2022, 2022.

570 Holton, J. R., Haynes, P. H., McIntyre, M. E., Douglass, A. R., Rood, R. B. and Pfister, L.:
571 Stratosphere-Troposphere exchange, *Reviews of Geophysics*, 33(4), 403–439,
572 doi:10.1029/95rg02097, 1995.

573 Homeyer, C. R. and Bowman, K. P.: Rossby Wave Breaking and Transport between the Tropics
574 and Extratropics above the Subtropical Jet, *Journal of the Atmospheric Sciences*, 70, 607–
575 626, <https://doi.org/10.1175/jas-d-12-0198.1>, 2013.

576 Hoskins, B. J. and Ambrizzi, T.: Rossby Wave Propagation on a Realistic Longitudinally
577 Varying Flow, *Journal of the Atmospheric Sciences*, 50, 1661–1671,
578 [https://doi.org/10.1175/1520-0469\(1993\)050<1661:rwpoar>2.0.co;2](https://doi.org/10.1175/1520-0469(1993)050<1661:rwpoar>2.0.co;2), 1993.

579 Iglesias-Suarez, F., Kinnison, D. E., Rap, A., Maycock, A. C., Wild, O. and Young, P. J.: Key
580 drivers of ozone change and its radiative forcing over the 21st century, *Atmospheric
581 Chemistry and Physics*, 18(9), 6121–6139, doi:10.5194/acp-18-6121-2018, 2018.

582 Kidston, J., Scaife, A. A., Hardiman, S. C., Mitchell, D. M., Butchart, N., Baldwin, M. P. and
583 Gray, L. J.: Stratospheric influence on tropospheric jet streams, storm tracks and Surface
584 Weather, *Nature Geoscience*, 8(6), 433–440, doi:10.1038/ngeo2424, 2015.

585 Kim, J., Park, H.-S., Son, S.-W., and Gerber, E. P.: Defining Sudden Stratospheric Warming in
586 Climate Models: Accounting for Biases in Model Climatologies, *Journal of Climate*, 30,
587 5529–5546, <https://doi.org/10.1175/jcli-d-16-0465.1>, 2017.

588 Knowland, K. E., Ott, L. E., Duncan, B. N. and Wargan, K.: Stratospheric intrusion-influenced
589 ozone air quality exceedances investigated in the NASA Merra-2 Reanalysis, *Geophysical
590 Research Letters*, 44(20), doi:10.1002/2017gl074532, 2017.

591 Kumar, V., Dhaka, S. K., Reddy, K. K., Gupta, A., Prasad, S. B. S., Panwar, V., Singh, N., Ho,
592 S.-P., and Takahashi, M.: Impact of quasi-biennial oscillation on the inter-annual variability
593 of the tropopause height and temperature in the tropics: A study using
594 COSMIC/FORMOSAT-3 observations, *Atmospheric Research*, 139, 62–70,
595 <https://doi.org/10.1016/j.atmosres.2013.12.014>, 2014.

596 Kumar, K. N., Sharma, S. K., Naja, M., and Phanikumar, D. V.: A Rossby wave breaking-
597 induced enhancement in the tropospheric ozone over the Central Himalayan region,
598 *Atmospheric Environment*, 224, 117356, <https://doi.org/10.1016/j.atmosenv.2020.117356>,
599 2020.

600 Kunz, A., Konopka, P., Müller, R. and Pan, L. L.: Dynamical tropopause based on isentropic
601 potential vorticity gradients, *Journal of Geophysical Research*, 116(D1),
602 doi:10.1029/2010jd014343, 2011.

603 Lee, J., Butler, A. H., Albers, J. R., Wu, Y. and Lee, S. H.: Impact of sudden stratospheric
604 warmings on the stratosphere-to-troposphere transport of ozone, *Geophysical Research
605 Letters*, 52(2), doi:10.1029/2024gl112588, 2025.

606 Li, H., Fan, Y., Li, Q., Ji, X., Zhang, J., and Sheng, B.: The Gravity Wave Activity during Two
607 Recent QBO Disruptions Revealed by U.S. High-Resolution Radiosonde Data, *Remote
608 Sensing*, 15, 472, <https://doi.org/10.3390/rs15020472>, 2023.

- 609 Li, Y., Xia, Y., Xie, F. and Yan, Y.: Influence of stratosphere-troposphere exchange on long-
610 term trends of surface ozone in CMIP6, *Atmospheric Research*, 297, 107086,
611 doi:10.1016/j.atmosres.2023.107086, 2024.
- 612 Lim, S. S., Vos, T., Flaxman, A. D., Danaei, G., Shibuya, K., Adair-Rohani, H., AlMazroa, M.
613 A., Amann, M., Anderson, H. R., Andrews, K. G., Aryee, M., Atkinson, C., Bacchus, L. J.,
614 Bahalim, A. N., Balakrishnan, K., Balmes, J., Barker-Collo, S., Baxter, A., Bell, M. L.,
615 Blore, J. D., Blyth, F., Bonner, C., Borges, G., Bourne, R., Boussinesq, M., Brauer, M.,
616 Brooks, P., Bruce, N. G., Brunekreef, B., Bryan-Hancock, C., Bucello, C., Buchbinder, R.,
617 Bull, F., Burnett, R. T., Byers, T. E., Calabria, B., Carapetis, J., Carnahan, E., Chafe, Z.,
618 Charlson, F., Chen, H., Chen, J. S., Cheng, A. T.-A., Child, J. C., Cohen, A., Colson, K. E.,
619 Cowie, B. C., Darby, S., Darling, S., Davis, A., Degenhardt, L., Dentener, F., Des Jarlais, D.
620 C., Devries, K., Dherani, M., Ding, E. L., Dorsey, E. R., Driscoll, T., Edmond, K., Ali, S. E.,
621 Engell, R. E., Erwin, P. J., Fahimi, S., Falder, G., Farzadfar, F., Ferrari, A., Finucane, M. M.,
622 Flaxman, S., Fowkes, F. G., Freedman, G., Freeman, M. K., Gakidou, E., Ghosh, S.,
623 Giovannucci, E., Gmel, G., Graham, K., Grainger, R., Grant, B., Gunnell, D., Gutierrez, H.
624 R., Hall, W., Hoek, H. W., Hogan, A., Hosgood, H. D., Hoy, D., Hu, H., Hubbell, B. J.,
625 Hutchings, S. J., Ibeanusi, S. E., Jacklyn, G. L., Jasrasaria, R., Jonas, J. B., Kan, H., Kanis, J.
626 A., Kassebaum, N., Kawakami, N., Khang, Y.-H., Khatibzadeh, S., Khoo, J.-P., et al.: A
627 comparative risk assessment of burden of disease and injury attributable to 67 risk factors
628 and risk factor clusters in 21 regions, 1990–2010: A systematic analysis for the global
629 burden of disease study 2010, *The Lancet*, 380(9859), 2224–2260, doi:10.1016/s0140-
630 6736(12)61766-8, 2012.
- 631 Lin, Y., Jiang, F., Zhao, J., Zhu, G., He, X., Ma, X., Li, S., Sabel, C. E. and Wang, H.: Impacts
632 of O₃ on premature mortality and crop yield loss across China, *Atmospheric Environment*,
633 194, 41–47, doi:10.1016/j.atmosenv.2018.09.024, 2018.
- 634 Liu, Y., Gao, S. T., Brasseur, G., Tie, X. X., Wang, H. P., Kinnison, D., and Liu, C. X.:
635 Atmospheric tracers during the 2003–2004 stratospheric warming event and impact of ozone
636 intrusions in the troposphere, *Atmospheric Chemistry and Physics*, 9, 2157–2170,
637 <https://doi.org/10.5194/acp-9-2157-2009>, 2009.
- 638 Ma, X., Huang, J., Hegglin, M., Joeckel, P. and Zhao, T.: Causes of growing middle-upper
639 tropospheric ozone over the Northwest Pacific Region, doi:10.5194/egusphere-2023-2411,
640 2024.
- 641 Myhre, G., & Stordal, F.: Role of spatial and temporal variations in the computation of radiative
642 forcing and GWP. *Journal of Geophysical Research: Atmospheres*, 102(D10), 11181–11200.
643 <https://doi.org/10.1029/97jd00148>, 1997.

644 Myhre, G., Shine, K. P., Rädcl, G., Gauss, M., Isaksen, I. S. A., Tang, Q., Prather, M. J.,
645 Williams, J. E., van Velthoven, P., Dessens, O., Koffi, B., Szopa, S., Hoor, P., Grewe, V.,
646 Borken-Kleefeld, J., Berntsen, T. K. and Fuglestvedt, J. S.: Radiative forcing due to changes
647 in ozone and methane caused by the transport sector, *Atmospheric Environment*, 45(2), 387–
648 394, doi:10.1016/j.atmosenv.2010.10.001, 2011.

649 Nowack, P. J., Luke Abraham, N., Maycock, A. C., Braesicke, P., Gregory, J. M., Joshi, M. M.,
650 Osprey, A. and Pyle, J. A.: A large ozone-circulation feedback and its implications for
651 global warming assessments, *Nature Climate Change*, 5(1), 41–45,
652 doi:10.1038/nclimate2451, 2014.

653 Park, C., Choi, J., Son, S., and Lim, Y.: Quasi-biennial oscillation-related surface air temperature
654 change over the western North Pacific in late winter, *International Journal of Climatology*,
655 42, 4351–4359, <https://doi.org/10.1002/joc.7470>, 2021.

656 Remya, R., Manoj, M. G., and Mohanakumar, K.: Role of Quasi-Biennial oscillation on the link
657 between sudden stratospheric warming and tropical weather events, *Advances in Space*
658 *Research*, 73, 571–584, <https://doi.org/10.1016/j.asr.2023.11.006>, 2023.

659 Roy, C., Thazhe Purayil, S., and Fadnavis, S.: The stratospheric ozone rich cold intrusion during
660 El-Nino over the Indian region: implication during the Indian summer monsoon,
661 <https://doi.org/10.5194/egusphere-egu2020-937>, 2020.

662 Roy, C., Ravishankara, A. R., Newman, P. A., David, L. M., Fadnavis, S., Rathod, S. D., Lait,
663 L., Krishnan, R., Clark, H. and Sauvage, B.: Estimation of stratospheric intrusions during
664 Indian Cyclones, *Journal of Geophysical Research: Atmospheres*, 128(3),
665 doi:10.1029/2022jd037519, 2023.

666 Scaife, A. A., Charlton-Perez, A. J., Son, S.-W., Hardiman, S. C., Polvani, L., Lim, E.-P.,
667 Haynes, P., Baldwin, M. P., Shepherd, T. G., Perlwitz, J., Richter, J. H., Noguchi, S.,
668 Thompson, D. W. J., Karpechko, A. Y., Butler, A. H., Scinocca, J., Sigmond, M., Domeisen,
669 D. Shi. V., and Garfinkel, C. I.: Long-range prediction and the stratosphere, *Atmospheric*
670 *Chemistry and Physics*, 22, 2601–2623, <https://doi.org/10.5194/acp-22-2601-2022>, 2022.

671 Schimanke, S., Spanghel, T., Huebener, H. and Cubasch, U.: Variability and trends of major
672 stratospheric warmings in simulations under constant and increasing GHG concentrations,
673 *Climate Dynamics*, 40(7–8), 1733–1747, doi:10.1007/s00382-012-1530-x, 2012.

674 Shell, K. M., Kiehl, J. T. and Shields, C. A.: Using the radiative kernel technique to calculate
675 climate feedbacks in NCAR’s community atmospheric model, *Journal of Climate*, 21(10),
676 2269–2282, doi:10.1175/2007jcli2044.1, 2008.

677 Shi, Y., Evtushevsky, O., Milinevsky, G., Wang, X., Klekociuk, A., Han, W., Grytsai, A., Wang,
678 Y., Wang, L., Novosyadlyj, B., and Andrienko, Y.: Impact of the 2018 major sudden
679 stratospheric warming on weather over the midlatitude regions of Eastern Europe and East
680 Asia, *Atmospheric Research*, 297, 107112, <https://doi.org/10.1016/j.atmosres.2023.107112>,
681 2023.

682 Sigmond, M., Scinocca, J. F., Kharin, V. V. and Shepherd, T. G.: Enhanced seasonal forecast
683 skill following stratospheric sudden warmings, *Nature Geoscience*, 6(2), 98–102,
684 doi:10.1038/ngeo1698, 2013.

685 Skeie, R. B., Myhre, G., Hodnebrog, Ø., Cameron-Smith, P. J., Deushi, M., Hegglin, M. I.,
686 Horowitz, L. W., Kramer, R. J., Michou, M., Mills, M. J., Olivie, D. J., Connor, F. M.,
687 Paynter, D., Samset, B. H., Sellar, A., Shindell, D., Takemura, T., Tilmes, S. and Wu, T.:
688 Historical total ozone radiative forcing derived from CMIP6 simulations, *npj Climate and
689 Atmospheric Science*, 3(1), doi:10.1038/s41612-020-00131-0, 2020.

690 SPARC Reanalysis Intercomparison Project (S-RIP) Final Report. M. Fujiwara, G.L. Manney,
691 L.J. Gray, and J.S. Wright (Eds.), SPARC Report No. 10, WCRP-17/2020, doi:
692 10.17874/800dee57d13, available at www.sparc-climate.org/publications/sparc-reports,
693 2022.

694 Sprenger, M., Croci Maspoli, M. and Wernli, H.: Tropopause folds and cross-Tropopause
695 Exchange: A global investigation based upon ECMWF analyses for the time period March
696 2000 to February 2001, *Journal of Geophysical Research: Atmospheres*, 108(D12),
697 doi:10.1029/2002jd002587, 2003.

698 Sprenger, M., Wernli, H. and Bourqui, M.: Stratosphere–troposphere exchange and its relation to
699 potential vorticity streamers and cutoffs near the extratropical tropopause, *Journal of the
700 Atmospheric Sciences*, 64(5), 1587–1602, doi:10.1175/jas3911.1, 2007.

701 Stamnes, K., Tsay, S.-C., Wiscombe, W. and Jayaweera, K.: Numerically stable algorithm for
702 discrete-ordinate-method radiative transfer in multiple scattering and emitting layered
703 media, *Applied Optics*, 27(12), 2502, doi:10.1364/ao.27.002502, 1988.

704 Wang, H., Lu, X., Jacob, D. J., Cooper, O. R., Chang, K.-L., Li, K., Gao, M., Liu, Y., Sheng, B.,
705 Wu, K., Wu, T., Zhang, J., Sauvage, B., Nédélec, P., Blot, R. and Fan, S.: Global
706 tropospheric ozone trends, attributions, and radiative impacts in 1995–2017: An integrated
707 analysis using aircraft (IAGOS) observations, ozonesonde, and multi-decadal chemical
708 model simulations, *Atmospheric Chemistry and Physics*, 22(20), 13753–13782,
709 doi:10.5194/acp-22-13753-2022, 2022.

710 Wang, M. and Fu, Q.: Stratosphere-troposphere exchange of Air Masses and ozone
711 concentrations based on reanalyses and observations, *Journal of Geophysical Research:*
712 *Atmospheres*, 126(18), doi:10.1029/2021jd035159, 2021.

713 Waugh, D. W. and Polvani, L. M.: Climatology of intrusions into the tropical upper troposphere,
714 *Geophysical Research Letters*, 27(23), 3857–3860, doi:10.1029/2000gl012250, 2000.

715 White, I. P., Lu, H., and Mitchell, N. J.: Seasonal evolution of the QBO-induced wave forcing
716 and circulation anomalies in the northern winter stratosphere, *Journal of Geophysical*
717 *Research: Atmospheres*, 121, 10,411–10,431, <https://doi.org/10.1002/2015jd024507>, 2016.

718 Williams, R. S., Hegglin, M. I., Jöckel, P., Garny, H. and Shine, K. P.: Air quality and radiative
719 impacts of downward-propagating sudden stratospheric warmings (ssws), *Atmospheric*
720 *Chemistry and Physics*, 24(2), 1389–1413, doi:10.5194/acp-24-1389-2024, 2024.

721 Williams, R. S., Hegglin, M. I., Kerridge, B. J., Jöckel, P., Latter, B. G., and Plummer, D. A.:
722 Characterising the seasonal and geographical variability in tropospheric ozone, stratospheric
723 influence and recent changes, *Atmospheric Chemistry and Physics*, 19(6), 3589–3620,
724 doi:10.5194/acp-19-3589-2019, 2019.

725 World Meteorological Organization (1957). *Meteorology—A three dimensional science: Second*
726 *session of the Commission for Aerology. WMO Bulletin*, IV(4), 134–138.

727 Xia, Y., Xie, F. and Lu, X.: Enhancement of Arctic surface ozone during the 2020–2021 winter
728 associated with the sudden stratospheric warming, *Environmental Research Letters*, 18(2),
729 024003, doi:10.1088/1748-9326/acae0, 2023.

730 Xia, Y., Huang, Y. and Hu, Y.: On the climate impacts of upper tropospheric and lower
731 stratospheric ozone, *Journal of Geophysical Research: Atmospheres*, 123(2), 730–739,
732 doi:10.1002/2017jd027398, 2018.

733 Zhang, J., Zhang, C., Zhang, K., Xu, M., Duan, J., Chipperfield, M. P., Feng, W., Zhao, S., and
734 Xie, F.: The role of chemical processes in the quasi-biennial oscillation (QBO) signal in
735 stratospheric ozone, *Atmospheric Environment*, 244, 117906,
736 <https://doi.org/10.1016/j.atmosenv.2020.117906>, 2020.

737 Ziemke, J. R., Chandra, S. and Bhartia, P. K.: “cloud slicing”: A new technique to derive upper
738 tropospheric ozone from satellite measurements, *Journal of Geophysical Research:*
739 *Atmospheres*, 106(D9), 9853–9867, doi:10.1029/2000jd900768, 2001.